J|A|C|S ARTICLES

Published on Web 03/03/2009

Transition State Distortion Energies Correlate with Activation Energies of 1,4-Dihydrogenations and Diels−Alder Cycloadditions of Aromatic Molecules

Amy E. Hayden and K. N. Houk*

Department of Chemistry and Biochemistry, University of California, Los Angeles, 607 Charles E. Young Drive, Los Angeles, California 90095-1569

Received November 22, 2008; E-mail: houk@chem.ucla.edu

Abstract: The reaction energetics of 43 1,4-dihydrogenation reactions of polycyclic aromatic hydrocarbons and nitrogen-containing heterocycles as well as the 43 analogous Diels−Alder reactions with ethylene (C_2H_4) have been computed using B3LYP/6-31G(d) density functional theory (DFT). The transition state distortion energies are found to correlate with the activation energies of these reactions, even for cases when energies of reaction do not correlate with reactivities.

Introduction

Models to understand and predict reactivity have long been a topic of interest in organic chemistry. In this Article, calculations on the uncatalyzed 1,4-additions of both dihydrogen and ethylene to series of polycyclic aromatic hydrocarbons (PAHs) (Figure 1)[1] and 6-membered nitrogen-containing heterocycles (Figure 2)[2] are examined. Radom et al. reported that the hydrogenations of these PAHs exhibit a linear relation between the activation enthalpies and the heats of reaction.[1] Such relationships have been referred to as Brønsted, Dimroth, Marcus, Bell−Evans−Polanyi, or the Bema Hapothle relationship.[2] However, this principle fails to correlate relative reactivities of these heterocycles in 1,4-hydrogenation reactions.[3]

In previous work in our group, it was discovered that distortion energy, the energy required to distort the reactants to the transition state geometry, is an important factor in controlling reactivity in several series of 1,3-dipolar cycloadditions for which the BEP principle fails.[4] We have now explored the reactions of 8 PAHs and 8 heterocycles with a total of 28 and 15 possible 1,4-addition modes, respectively. The reactions of both H_2 and C_2H_4 with these 16 molecules provide a large data set (86 reactions) for testing the distortion-interaction model. PAHs, especially pentacene and higher order acenes, and their reactivities are of interest in various organic semiconductor applications.[5]

The 1,4-additions to PAHs were first observed over 60 years ago by Clar[6] and by Diels and Alder.[7] Clar also observed that

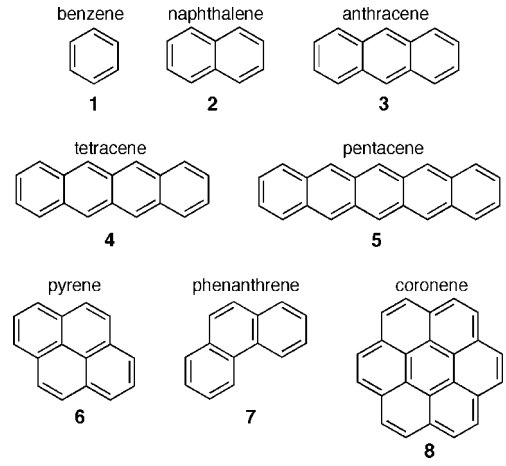

Figure 1. Linear and branched PAHs.

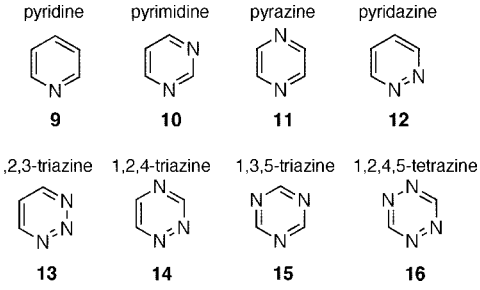

Figure 2. Nitrogen-containing heterocycles.

the reactivity of the PAH increases with linear annelation (i.e., from benzene **1** to pentacene **5**, Figure 1) and decreases with nonlinear (angular) annelation (i.e., naphthalene **2** as compared to phenanthrene **7**).[8]

Several models have been applied to this PAH reactivity pattern. Brown proposed that para-localization energy, computed

(1) Zhong, G.; Chan, B.; Radom, L. *THEOCHEM* **2007**, *811*, 13–17.
(2) Jencks, W. P. *Chem. Rev.* **1985**, *85*, 511–527.
(3) Zhong, G.; Chan, B.; Radom, L. *J. Am. Chem. Soc.* **2007**, *129*, 924–933.
(4) (a) Ess, D. H.; Houk, K. N. *J. Am. Chem. Soc.* **2007**, *129*, 10646–10647. (b) Ess, D. H.; Houk, K. N. *J. Am. Chem. Soc.* **2008**, *130*, 10187–10198. (c) Jones, G. O.; Houk, K. N. *J. Org. Chem.* **2008**, *73*, 1333–1342.
(5) Pope, M.; Swernberg, C. E. *Electronic Processes in Organic Crystals and Polymers*, 2nd ed.; Oxford University Press: Oxford, 1999; pp 337−340.
(6) Clar, E. *Ber. Dtsch. Chem. Ges.* **1931**, *64*, 1682.
(7) Diels, O.; Alder, K. *Justus Liebigs Ann. Chem.* **1931**, *486*, 191.
(8) Clar, E. *Ber. Dtsch. Chem. Ges.* **1939**, *72*, 1817.

10.1021/ja809142x CCC: $40.75

Figure 3. Illustration of the nomenclature used for 1,4-addition to PAHs.

from Hückel theory, is related to the ease of formation of product.[9] This theory fails with certain substitutions as well as for higher order acenes.[10] Second-order perturbation theory has been used, but has similar limitations.[11] Free valences from Hückel theory are applicable when the reactions under study have relatively early transition states.[12] Hess−Schaad resonance energies[13] correlated with reactivity with certain data sets.[14] Herndon demonstrated a linear relationship between experimentally obtained free energies of activation and computed resonance energies for some Diels−Alder reactions.[15] Schmidt and co-workers successfully correlated several of the aforementioned methods with spectroscopic data using acenes and benzologs,[16] phenes and starphenes,[10] and additional PAHs[17] as test sets, but which model correlated well was dependent upon the test set used.

Another theory that faces limitations for these reactions is frontier molecular orbital (FMO) theory. Although FMO theory[18] has found wide use in organic chemistry,[19] it fails in predicting the reactivity of PAHs. Schmidt notes that benzene is predicted by FMO theory to be more reactive to 1,4-addition than is hexacene,[16] which is exactly the opposite of what is observed and predicted with theoretical methods.

In an attempt to explain his earlier observations, Clar attributed the phenomenon of increasing reactivity with increasing acene length to the gradual loss of benzenoid (aromatic) character using his sextet theory.[20] Polansky and Derflinger subsequently constructed a quantitative model of Clar's theory.[21] More recently, however, Schleyer et al. have computed nucleus-independent chemical shifts (NICS) to probe the aromaticity of various aromatic systems.[22] Both Cyrański[23] and Schleyer[24] have demonstrated relationships between reactivity and aromatic stabilization for PAHs using computed NICS values: higher order PAHs do not have a decreasing benzenoid character, which contradicts Clar's earlier sextet theory. In fact, the innermost ring of the molecule, which is actually the most reactive ring, is also the most aromatic, while the least reactive outermost rings are the least aromatic. The reaction energetics for Diels−Alder reactions of five linear PAHs (benzene through pentacene) with acetylene were studied, and the reactivity trend was attributed by Schleyer to the BEP principle.[25] Cheng and Li reported similar findings when theoretically examining the Diels−Alder reactions of linear PAHs with ethylene.[26]

This Article reports computations on the reactions of PAHs and nitrogen-containing heterocycles with H_2 and C_2H_4 using the same sets of molecules studied by Radom.[1,3] The activation barriers are compared to reaction energies and distortion energies in the transition state in the first part of the Article, then the geometries of the transition states are described, and the positions of the transition states are analyzed. Finally, we describe the origins of the correlations between distortion and activation energies.

Computational Methods

All calculations were performed with Gaussian 03[27] using the density functional B3LYP with the 6-31G(d) basis set. To verify that this method was sufficiently accurate when compared to the method used by Radom (MPWB1K/6-311+G(3df,2p)//B3LYP/6-31G+(d)),[1] Radom's MPWB1K values and the B3LYP/6-31G(d) energies were plotted against each other, revealing a linear plot with slopes of approximately 1 (for activation energies, $\Delta H^{\ddagger}$ (B3LYP) = 0.97$\Delta H^{\ddagger}$ (MPW1K) − 0.94, R^2 = 0.998; for reaction energies, ΔH (B3LYP) = 1.0ΔH (MPW1K) − 4.3, R^2 = 0.997). The excellent agreement between the B3LYP results with a small basis set and Radom's more time-consuming calculations encouraged the use of B3LYP/6-31G(d) throughout this work. See the Supporting Information for more details. Vibrational frequencies were computed for all optimized structures to verify that they were either minima or transition states. Distortion energies were then computed by performing a single point energy calculation using B3LYP/6-31G(d) on each of the separated, distorted fragments. Throughout this Article, energies and distances are given in kcal/mol and angstroms, respectively.

Results and Discussion

The Radom system of nomenclature[1,3] is used in this Article: each reacting position of the PAH is classified by the number of rings that share a carbon at that junction (Figure 3). Thus, there are [1,1], [1,2], [2,2], [1,3], and [3,3] modes of 1,4-addition. In general, the more ring junctions are at the reacting positions, the higher are the activation and corresponding product energies (see Figure 8 for an illustration of this principle). A large range of energies is possible in a set of seemingly similar reactions because of the large variety of types of possible reaction positions. In the case of the nitrogen-containing heterocycles, there are three possible modes of reactions: [C,C], [C,N], and [N,N]. The C or N in this notation indicates the atom types at which the H_2 or C_2H_4 is reacting.

A number of models have shown that for many reactions $\Delta\Delta G^{\ddagger} = 1/2\Delta\Delta G_{rxn}$.[28] For example, the Hammond−Leffler postulate indicates that slopes <0.5 indicate earlier, reactant-like transition states, while >0.5 slopes indicate later, product-like transition states.[29] In Marcus theory, this relationship arises for reactions that are not very exothermic or endothermic. Figure 4 shows a curve predicted by Marcus theory for the reaction of arenes with H_2. The plotted points are nearly linear, but a slight parabolic curve is observable.

(9) Brown, R. D. *J. Chem. Soc.* **1950**, 691–697.
(10) Biermann, D.; Schmidt, W. *J. Am. Chem. Soc.* **1980**, *102*, 3173–3181.
(11) Clark, P. A.; Brogli, F.; Heilbronner, E. *Helv. Chim. Acta* **1972**, *55*, 1415.
(12) Pullman, B.; Pullman, A. *Prog. Org. Chem.* **1958**, 4.
(13) Hess, B. A.; Schaad, L. J. *J. Am. Chem. Soc.* **1971**, *93*, 305–310.
(14) Wightman, R. H.; Cresp, T. M.; Sondheimer, F. *J. Am. Chem. Soc.* **1976**, *98*, 6052–6053.
(15) Herndon, W. C. *J. Chem. Soc., Chem. Commun.* **1977**, 817–818.
(16) Biermann, D.; Schmidt, W. *J. Am. Chem. Soc.* **1980**, *102*, 3163–3173.
(17) Hess, B. A.; Schaad, L. J.; Herndon, W. C.; Biermann, D.; Schmidt, W. J. *Tetrahedron* **1981**, *37*, 2983–2987.
(18) Fukui, K. *Fortschr. Chem. Forsch.* **1970**, *15*, 1–85.
(19) (a) Houk, K. N. *Acc. Chem. Res.* **1975**, *8*, 361–369. (b) Geittner, J.; Huisgen, R.; Sustmann, R. *Tetrahedron Lett.* **1977**, *10*, 881–884.
(20) (a) Clar, E. *Polycyclic Aromatic Hydrocarbons*; Academic Press: New York, 1964. (b) Clar, E. *The Aromatic Sextet*; Wiley: New York, 1972.
(21) Polansky, O. E.; Derflinger, G. *Int. J. Quantum Chem.* **1967**, *1*, 379–401.
(22) Schleyer, P. v. R.; Maerker, C.; Dransfield, A.; Jiao, H.; Hommes, N. J. R. v. E. *J. Am. Chem. Soc.* **1996**, *118*, 6317–6318.
(23) Cryański, M. K.; Stępień, B. T.; Krygowski, T. M. *Tetrahedron* **2000**, *56*, 9663–9667.
(24) Schleyer, P. v. R.; Manoharan, M.; Jiao, H.; Stahl, F. *Org. Lett.* **2001**, *3*, 3643–3646.
(25) (a) Bell, R. P. *Proc. R. Soc. London, Ser. A* **1936**, *154*, 414–429. (b) Evans, M. G.; Polanyi, M. *Trans. Faraday Soc.* **1938**, *34*, 11.
(26) Cheng, M.-F.; Li, W.-K. *Chem. Phys. Lett.* **2003**, *368*, 630–638.
(27) Frisch, M. J. *Gaussian 03*, revision C.02; Gaussian, Inc.: Wallingford, CT, 2004.

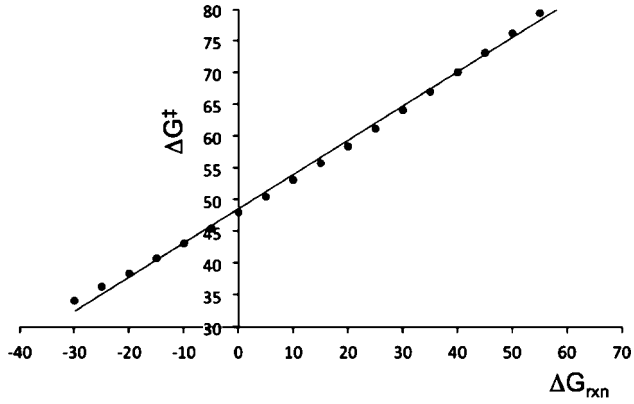

Figure 4. Theoretical Marcus curve for the range of reaction energies computed for the reactions of PAHs and dihydrogen. The data points are derived from $\Delta G^{\ddagger} = \Delta G_0^{\ddagger} + 1/2\Delta G_{rxn} + \Delta G^2_{rxn}/16\Delta G_0^{\ddagger}$, and the least-squares line has the equation $\Delta G^{\ddagger} = 0.54\Delta G_{rxn} + 49$. $\Delta G_0^{\ddagger}$ is 48 kcal/mol for $\Delta G_{rxn} = 0$ kcal/mol.

When reactions have similar values of $\Delta S^{\ddagger}$, then $\Delta\Delta H^{\ddagger} = 1/2\Delta\Delta H_{rxn}$ as well. This is found to hold true for both the hydrogenation (Figure 5a) and the Diels−Alder reactions (Figure 5b) of hydrocarbons, with slopes of 0.52 and 0.51, respectively. The slopes here are nearly constant, even though the reactions all vary from exothermic ($\Delta H_{rxn} \approx -20$ kcal/mol) to very endothermic ($\Delta H_{rxn} \approx 70$ kcal/mol).

For the reactions of the heterocycles with H_2, there is no obvious overall correlation (Figure 5c). There are correlations for the same reaction modes, [C,N] and [N,N], but the slopes are between 0.8 and 0.9. Moreover, the reactions occurring in the [C,C] mode have a very poor correlation ($R^2 = 0.629$). On the other hand, the analogous reactions of these heterocycles with C_2H_4 do give linear BEP plots (Figure 5d), but still have a slope of 0.9. All four sets of data are placed on the same plot in Figure 5e. It is clear that there is only a general trend rather than a quantitative BEP correlation.

We also explored whether there is a relationship between the activation energies and distortion energies, as was found recently

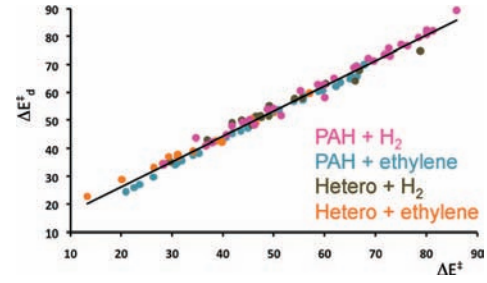

Figure 6. The relationship of the distortion energy in the transition state versus the activation energy in the transition state for all four data sets ($\Delta E^{\ddagger} = 0.90\Delta E^{\ddagger}_{dist} + 8.2$, $R^2 = 0.987$). Energies are given in kcal/mol (B3LYP/6-31G(d)).

for 1,3-dipolar cycloaddition reactions,[4] and as was briefly discussed by Radom et al.[1] Distortion energy is defined as the energy required to distort the reactants from their initial geometries to their transition state geometries, while the interaction energy is the binding energy between these reacting fragments in their transition state geometries. Morokuma first discussed these concepts when defining the activation energy as the sum of the "deformation" energy and the interaction energy.[30] Houk and co-workers also discussed how these distortions of reactants are required to achieve orbital interactions in transition states of cycloadditions.[31] More recently, Houk and Ess demonstrated a good linear correlation between activation energy ($\Delta E^{\ddagger}$) and distortion energy in the transition state ($\Delta E^{\ddagger}_d$) for 18 1,3-dipolar cycloadditions.[4a] Burnell et al. earlier discussed how distortion energies influence syn/anti-stereoselectivities in Diels−Alder reactions.[32]

The calculated distortion energies for all of these hydrogenation and ethylene Diels−Alder reactions are plotted against the activation energy in Figure 6. A linear correlation is found even when including all of the reactions, with a slope of 0.90 and $R^2 = 0.987$. The other quantity obtained from these calculations is the interaction energy in the transition state. The interaction energies are quite small in magnitude (~0.5−6.5 kcal/mol) when compared to the distortion energies (~25−90 kcal/mol). Some

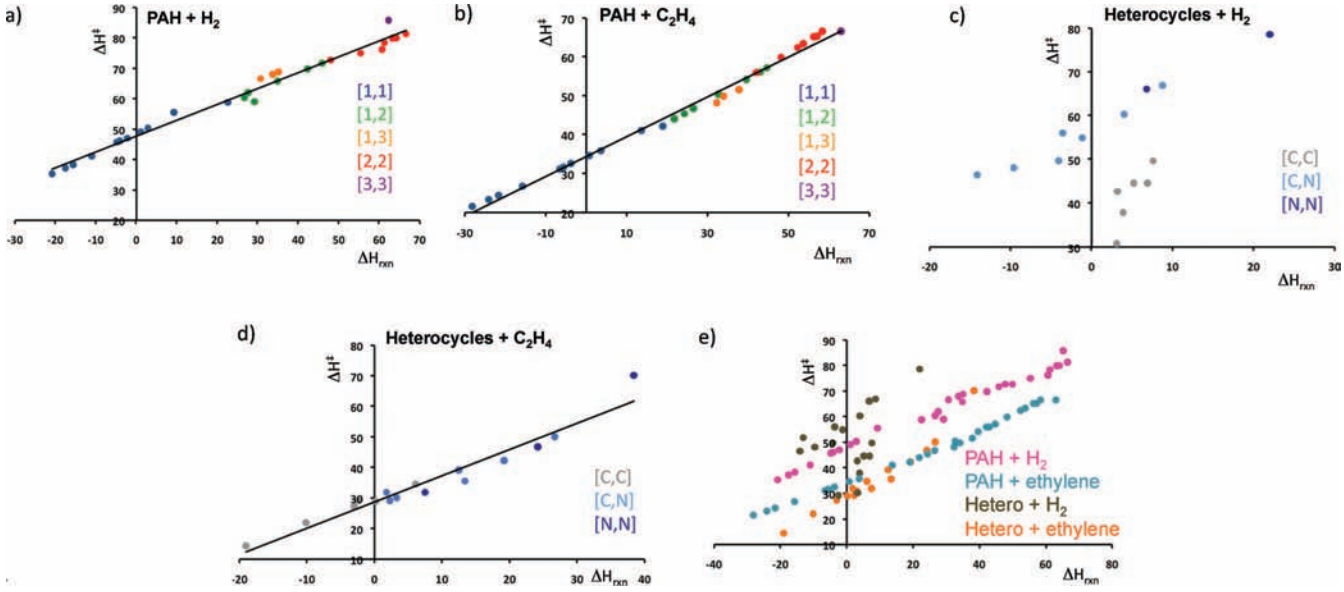

Figure 5. BEP plots of the reactions of (a) PAHs with H_2 ($\Delta H^{\ddagger} = 0.52\Delta H_{rxn} + 48$, $R^2 = 0.982$), (b) PAHs with ethylene ($\Delta H^{\ddagger} = 0.51\Delta H_{rxn} + 34$, $R^2 = 0.984$), (c) heterocycles with H_2 ([C,C], $\Delta H^{\ddagger} = 2.7\Delta H_{rxn} + 28$, $R^2 = 0.629$; [C,N], $\Delta H^{\ddagger} = 0.90\Delta H_{rxn} + 57$, $R^2 = 0.910$; [N,N], $\Delta H^{\ddagger} = 0.98\Delta H_{rxn} + 1.5$, $R^2 = 0.995$; overall, $\Delta H^{\ddagger} = 0.69\Delta H_{rxn} + 50$, $R^2 = 0.226$), and (d) heterocycles with ethylene ($\Delta H^{\ddagger} = 0.86\Delta H_{rxn} + 29$, $R^2 = 0.941$). (e) All four sets of data shown on the same plot. In the first four graphs, different modes of reaction are shown in different colors, as indicated. In (e), each data set is color-coded, as indicated in the key. All enthalpies are given in kcal/mol (B3LYP/6-31G(d)).

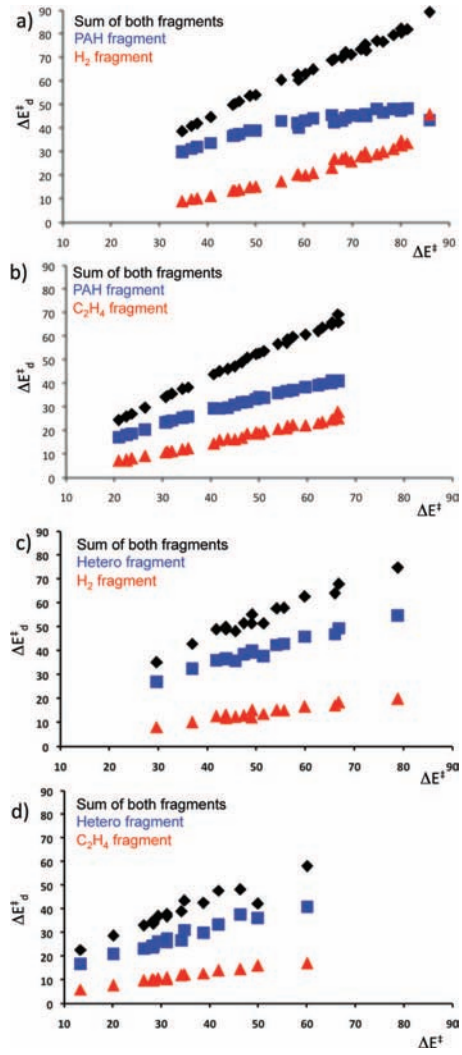

Figure 7. Total transition state distortion energies and corresponding distortion energies of the individual fragments plotted against the energy: (a) PAH and H_2 reactions, (b) PAH and ethylene reactions, (c) heterocycle and H_2 reactions, and (d) heterocycle and ethylene reactions. All energies are in kcal/mol (B3LYP/6-31G(d)). Linear equations are found in the Supporting Information.

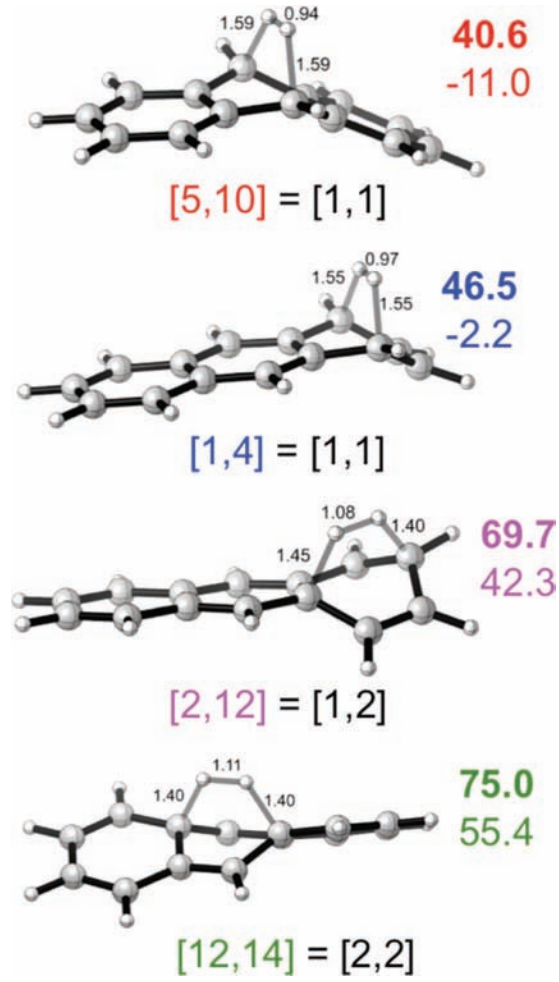

Figure 8. Transition states for the four reactions of H_2 with anthracene. Below each structure is shown: position of reaction = mode of reaction. To the right is the corresponding activation (bold) and reaction energies in kcal/mol (B3LYP/6-31G(d)). Bond lengths are given in angstroms.

of the points deviate from the line in Figure 6 by a considerable amount (up to ~8 kcal/mol), but the overall correlation is very good, as indicated by the R^2 value. The correlation described here shows that reactions that follow the BEP principle also give correlations between $\Delta E^{\ddagger}$ and $\Delta E^{\ddagger}_{d}$. Of considerable interest is the fact that reactions that do not obey the BEP principle, such as the 1,3-dipolar cycloadditions described earlier[4] and the 1,4-H_2 addition to nitrogen heterocycles, still show correlations between $\Delta H^{\ddagger}$ and $\Delta H^{\ddagger}_{d}$.

The distortion energies presented in Figure 6 are the sums of the distortion energies of both reacting fragments. The distortion energies of each reactant can also be examined separately. For each reaction, the distortion energy of each fragment is also proportional to the activation energy. Figure 7 illustrates the individual distortion energies of each fragment. In each of the four data sets, the larger PAH or heterocycle (blue) fragment contributes more distortion energy than does the smaller H_2 or C_2H_4 fragment (red). In general, the distortion energy of both fragments increases with increasing total distortion energy.

A general trend seen in computed data is that reactions with lower activation energies have higher interaction energies. However, no hard and fast correlation is seen with these values (see the Supporting Information for a plot of $\Delta E^{\ddagger}_{int}$ vs $\Delta E^{\ddagger}$), presumably because the interaction energy has many components that have not been separated here including electrostatic, polarization, exchange repulsion, and charge transfer terms.[30]

Figure 8 provides some examples of transition state geometries that occur for one PAH reacting with H_2. The higher the activation energy and more endothermic the reaction, the later the transition state, as is evidenced by the longer breaking H−H bond as well as the shorter C−H forming bond distances, in agreement with the Hammond−Leffler postulate.

(28) (a) Hammond, G. S. *J. Am. Chem. Soc.* **1955**, *77*, 334–338. (b) Marcus, R. A. *Annu. Rev. Phys. Chem.* **1964**, *15*, 155–196.
(29) Pross, A. *Theoretical and Physical Principles in Organic Reactivity*; Wiley: New York, 1995.
(30) (a) Nagase, S.; Morokuma, K. *J. Am. Chem. Soc.* **1978**, *100*, 1666–1672. (b) Froese, R. D. J.; Coxon, J. M.; West, S. C.; Morokuma, K. *J. Org. Chem.* **1997**, *62*, 6991–6996.
(31) Houk, K. N.; Gandour, R. W.; Strozier, R. W.; Rondan, N. G.; Paquette, L. A. *J. Am. Chem. Soc.* **1979**, *101*, 6797–6802.
(32) Xidos, J. D.; Poirier, R. A.; Pye, C. C.; Burnell, D. J. *J. Org. Chem.* **1998**, *63*, 105–112.

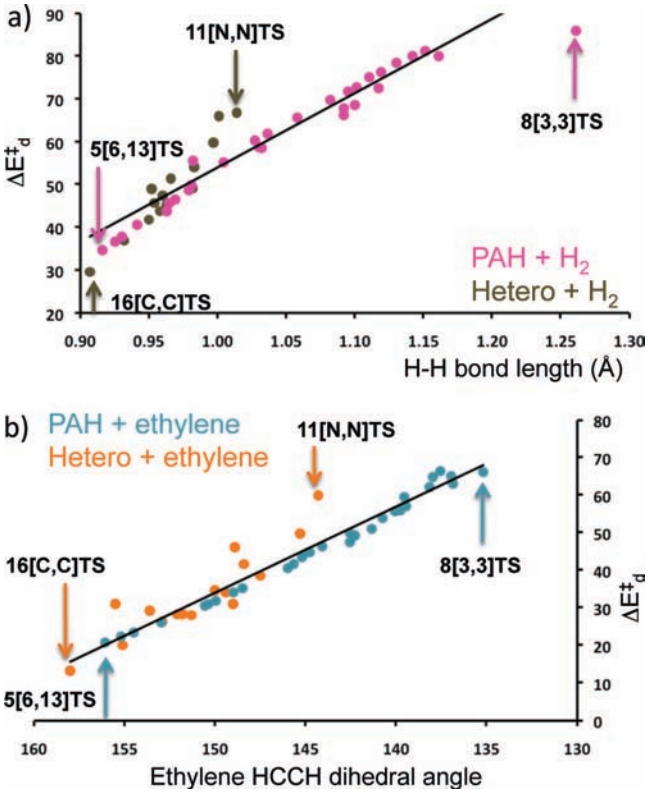

Figure 9. Relationships between transition state geometry and distortion energy. (a) Distortion energy of H_2 fragment in the transition state versus H−H bond length. (b) Distortion energy of the ethylene fragment in the transition state versus H−C−C−H dihedral angle.

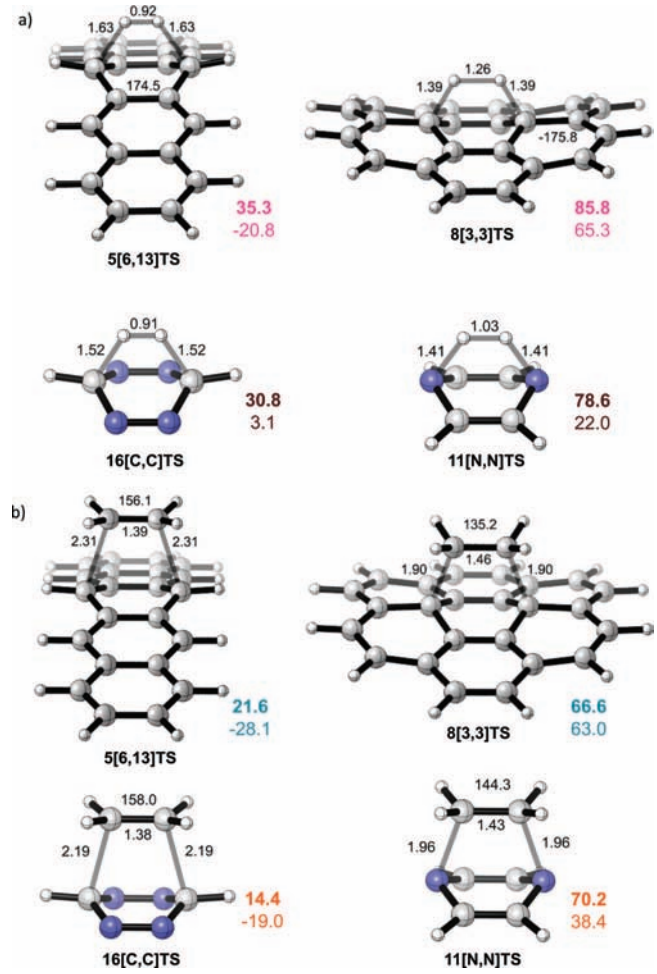

Figure 10. Transition state geometries of the points indicated on the graphs in Figure 9 for reactions with (a) hydrogen and (b) ethylene. To the right is the corresponding activation (bold) and reaction energies in kcal/mol (B3LYP/6-31G(d)). Bond lengths are given in angstroms.

This trend is found to be general for all reactions examined and can be quantified using the H−H distance in the transition state for 1,4-dihydrogenation reactions (Figure 9a, $R^2 = 0.887$) and the *trans*-H−C−C−H dihedral angle of C_2H_4 (Figure 9c, $R^2 = 0.938$) in the transition state for the Diels−Alder reactions. Increasing the H−H or C−C distance or distorting the ethylene fragment from planarity results in higher distortion energies. Figure 10 shows the lowest and highest energy transition structures for each data set, which are indicated on each graph in Figure 9. These three geometric parameters are linearly related to distortion energy. Therefore, as a consequence of the relation in Figure 6, these bond lengths and angles are also related to the activation energy. The forming bond distances were not used in this analysis only because many of the reactions are asynchronous, rendering two forming bond distances of differing lengths.

The distortion and interaction energies have been examined along the intrinsic reaction coordinate (IRC) for these reactions (Figure 11). At the transition state ($x = 0$), the derivative of the distortion energy is equal and opposite in sign to the derivative of the interaction energy. The transition state is often at the point where the interaction energy changes from repulsive to stabilizing. Qualitatively, the reactants must distort to a point along the reaction coordinate where the overlap between reactant orbitals becomes stabilizing.[31] In Figure 11, the interaction energy is near zero at each transition state, or somewhat negative for tetrazine reactions. Further motion along the reaction coordinate leads to substantial stabilization through the formation of bonds.

These reactions do not involve major stabilizing HOMO−LUMO interactions between reactants until substantial distortion occurs and the orbitals of the two reactants are well-aligned for overlap leading to bonding. Consequently, the activation energy approximately equals the distortion energy. In other cases, such as the 1,3-dipolar cycloadditions, interaction energies are stabilizing at the transition state due to favorable HOMO−LUMO interactions.[4]

Why do distortion energies always correlate with activation energies, but the energies of reaction may or may not correlate? Figure 12 describes these relations in terms of a Marcus theory-type overlay of parabolas representing distortion of reactants and products along the reaction coordinate. On the left, a thermoneutral reaction is represented. In the central diagram, the product parabola has been shifted downward, but the force constant of the product is maintained. This will result in a correlation of the activation energy with both the distortion energy and the reaction energy. Such reactions include addition of dihydrogen and ethylene to PAHs and the reaction of ethylene with nitrogen heterocycles. On the right, the energy of the product is shifted downward, and the force constant of the product is changed. The activation energy will still have a correlation with the distortion energy, but not the reaction energy (such as the reaction of nitrogen heterocycles with dihydrogen). $\Delta E^{\ddagger}_{d}$ is always close to $\Delta E^{\ddagger}$, so changes are also similar, while ΔE_{rxn} may vary considerably.

We also tested if the product distortion energy might correlate with $\Delta E^{\ddagger}$. Distortion energy of the products (ΔE_d) is analogous to $\Delta E^{\ddagger}_{d}$, except that the energy required to distort from the initial

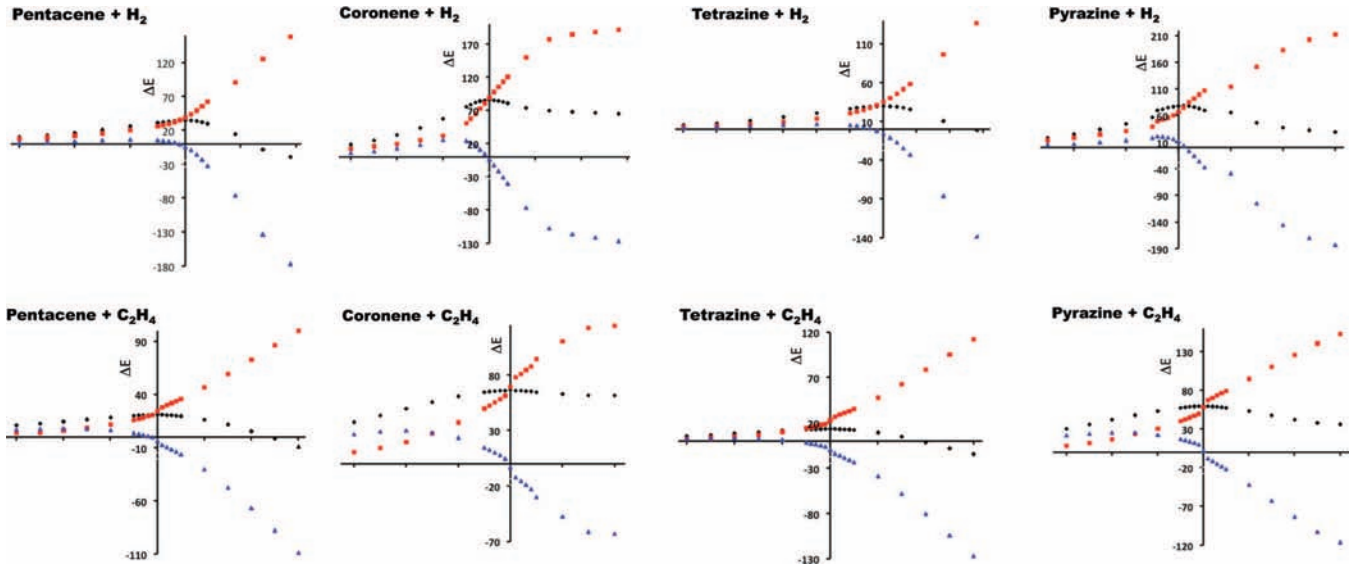

Figure 11. Total energy (black), distortion energy (red), and interaction energy (blue) along the reaction coordinate for the reaction of pentacene with H_2 and C_2H_4 at the [6,13] position, coronene with H_2 and C_2H_4 in the [3,3] reaction mode, tetrazine with H_2 and C_2H_4 in the [C,C] reaction mode, and pyrazine and H_2 and C_2H_4 in the [N,N] reaction mode. Transition states are at $x = 0$. Structures of the end points of each of these plots are in the Supporting Information. Energies are given in kcal/mol (B3LYP/6-31G(d)).

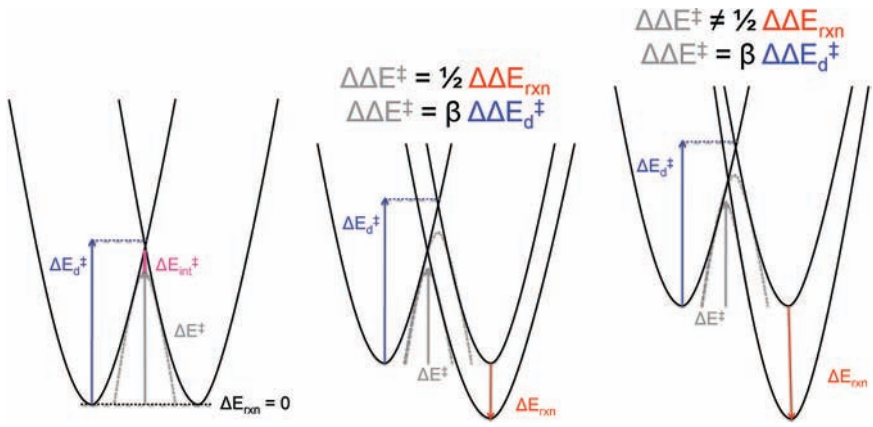

Figure 12. An equienergy tranformation demonstrating the key energetic quantities (left), reactions that follow both the distortion/interaction model and the BEP principle (middle), and reactions that follow the distortion/interaction model but not the BEP principle (right).

reactant geometry is computed using the product geometry instead of the transition state geometry. Little, if any, correlation is seen between distortion energy in the transition state and distortion energy in the product (see Supporting Information for a graph of these data).

Conclusions

$\Delta E^{\ddagger}$ often correlates with ΔE_{rxn} for 1,4-addition reactions, but this is dependent upon the specific reactions under study. For example, for the 1,4-addition of dihydrogen to a series of nitrogen heterocycles, no correlation is seen between $\Delta E^{\ddagger}$ and ΔE_{rxn}, but a correlation between these quantities is observed for the Diels−Alder reaction of these same heterocycles with ethylene as well as the 1,4-addition reactions of PAHs with dihydrogen and ethylene. However, the correlation with $\Delta E^{\ddagger}$ and $\Delta E^{\ddagger}_{d}$ has been demonstrated to be more general than $\Delta E^{\ddagger}$ and ΔE_{rxn} for 1,4-addition reactions, showing the same relationship between $\Delta E^{\ddagger}$ and $\Delta E^{\ddagger}_{d}$ for all reactions studied in this Article. In addition, the distortion and interaction energies have been examined along the reaction coordinate, and it was found that the transition state is generally where the interaction energy changes from repulsive to stabilizing.

Acknowledgment. We are grateful to the National Science Foundation for financial support. A.E.H. acknowledges a traineeship (NSF IGERT: Materials Creation Training Program) and the UCLA Dissertation Year Fellowship. The computations were performed using the UCLA Academic Technology Services (ATS) Hoffman Beowulf cluster as well as the California NanoSystems Institute (CNSI) Beowulf cluster.

Supporting Information Available: Method comparison details, linear equations of plotted data, examination of interaction energy in the transition state when compared to activation energy, a discussion of the product interaction energy, structures of the end points of the IRCs, complete ref 27, absolute and relative energies, and Cartesian coordinates of stationary points. This material is available free of charge via the Internet at http://pubs.acs.org.

JA809142X